Surface Chemistry Induced by High Energy Radiation in Silica of Small Particle Structures

Guohong Zhang, Yun Mao,† and J. Kerry Thomas*

Department of Chemistry and Biochemistry, University of Notre Dame, Notre Dame, Indiana 46556

Received: March 28, 1997; In Final Form: June 11, 1997[⊗]

Spectroscopic techniques are used to investigate energy transfer and radiation-induced reactions on the surfaces of particulate silicas. Upon subjection to high energy radiation, hydrogen atoms are produced with significant yields in all silica samples pretreated at 150 °C, for an example, $G(H) = 4.2$ in silica gel Davisil 60. Subsequent hydrogen addition to aromatic adsorbates such as pyrene, *N*,*N*-dimethylaniline, and methyl viologen (MV^{2+}) proceeds on the surface in competition with the hydrogen dimerization, leading to the formation of their H adducts. Hydrogen scavenging studies revealed that such addition reactions are heterogeneous in porous silica gel with contributions from a fast intrapore reaction within several nanoseconds and a much slower diffusion influenced interpore process over many microseconds. The efficient capture of H atoms by pyrene at a small percentage of surface coverage suggests that hydrogen is produced at the specific sites where pyrene adsorbs. Electron scavenging by $CHCl_3$, Cd^{2+}, and MV^{2+} leads to a suppression of H addition and an enhanced positive charge transfer to pyrene. Pretreatment of silica samples at 600 °C gives rise to increased ionic products of aromatic adsorbates, concomitant with decreased hydrogen production. These experimental observations are understood in terms of an exciton model. By comparison with the electronic processes in bulk silica materials, it is shown that surface plays a major role in the relaxation of excitation and the activation of adsorbate chemistry.

Introduction

Reactions on solid surfaces induced by photon and high-energy radiation are of particular interest from the perspective of both materials science and catalysis. However, in contrast to its extensive development in gas and liquid phases in the last thirty years, radiation chemistry in heterogeneous solid systems is far from well established. Early radiation studies of high surface area oxides, such as silicas, aluminas, zeolites, and other metal oxides, were carried out in the steady-state mode. It was found that excitation energy is transferred from solid particles to solid surfaces, and significant chemistry occurs at interfaces.[1] The reactions studied include oxidation and decomposition of organic adsorbates and polymerization of various vinyl monomers.[2−7] Reactive intermediates and reaction mechanisms involved in the chemical reactivity of the above solid systems are not clearly understood, except for some tentative propositions drawn from the analysis of final products. Detailed knowledge of the formation of transient intermediates and the structure−property relationship for these solids is essential in the design and preparation of specific catalysts.

High surface area silica, as one of the most widely used catalyst supports, is always the subject of interest and of experimental studies.[8−18] The recent success in photochemical studies in this particular area has provided us a much better understanding of silica and related systems than that which was available in the early days. New approaches to the radiation chemistry of solid surfaces include improvement in sample preparation and utilization of time-resolved spectroscopic techniques.[19,20] Molecular probing techniques, which make use of the characteristic reactions and spectroscopic properties of probe molecules, have been successfully applied to characterize electronic interactions in a variety of heterogeneous systems.[21,22] By using pyrene and methyl viologen as spectroscopic probes, our recent work shows that high-energy irradiation leads to efficient charge trapping and charge transfer reactions in both dehydrated and hydrated zeolites.[23] Of particular importance, it was found that the trapping of electrons in the conduction band by nanometer water clusters confined in the zeolite cages gives rise to the formation of solvated electrons. Meanwhile, oxidation of adsorbed water by the positive holes in the zeolite framework produces a large yield of hydroxyl radicals. The same conceptual and experimental approaches used in the above studies are now applied to silica surfaces.

Early work using electron spin resonance (ESR) techniques indicated that the hydroxyl groups on silica surfaces are dissociated by γ-radiolysis, leading to the formation of highly reactive hydrogen atoms which initiate further free radical reactions.[8,9] Due to the loss of surface hydroxyls in this way, silica gel generally exhibits significantly decreased adsorptivity of water and organic compounds after high-energy irradiation.[10] Radiation-induced chemical reactivity of silica gel draws particular attention because of its potential applications in catalysis. Pretreatment temperature was found to be the most important factor in the generation of catalytic activity by ionizing radiation. Silica dried at 150∼200 °C is normally inert, showing no chemistry upon irradiation other than hydrogen production. Extensive work on silica gel activated at temperatures above 500 °C indicated that stable acidic centers are produced on an irradiated silica surface.[11,12] These acidic centers are responsible for the observed surface reactions such as carbonium ion formation, polymerization of adsorbed monomers, dealkylation of isopropylbenzene, and decomposition of alkanes and alcohols. The term "energy transfer" was generally used to describe the activation of adsorbates which initiates subsequent surface reactions.[1] Experiments have also been performed at low temperatures to interrogate the transient intermediates involved in the above surface reactions. The presence of radical ions of organic adsorbates suggests that energy transfer might proceed via charge transfer reactions between charge-accepting and charge-donating centers formed on silica surfaces during ir-

* Author to whom correspondence should be addressed.
† Present address: 1 Cyclotron Road, Lawrence Berkeley Laboratory, MS 70A−3307, Berkeley, CA 94720.
⊗ Abstract published in *Advance ACS Abstracts,* August 15, 1997.

S1089-5647(97)01102-4 CCC: $14.00

radiation and organic adsorbates.[13,14] In spite of these important experimental findings, previous work has failed to provide a clear and unified understanding of the structure of reactive centers, the formation of various primary intermediates, and the effects of surface hydroxylation on chemical reactivity.

Further examination of model silica systems also provides a comparative insight for silica−alumina and alumna systems due to their structural similarity.[3,11] Recent work from this laboratory has identified the formation of adsorbate cation radicals on an irradiated silica−alumina surface, but left an unknown free radical intermediate unexplained.[24] In the present study, pyrene is again used as one of the spectroscopic probes to characterize guest−host interactions and reactive intermediates in real time. In addition to the well-established properties of the excited states and the ion radicals of pyrene, a free radical intermediate of pyrene, namely 1-hydropyrenyl radical (PyH•), the product of a hydrogen addition reaction, was also identified. This species was characterized in our earlier pulse radiolysis study of liquid methanol.[25] The formation of this H adduct radical in high-energy irradiation of silicas is identified and attributed to hydrogen atom addition reaction on these surfaces. Quantitative measurements of the production of pyrene free radicals and ion radicals were made on silica surfaces pretreated at different temperatures. In comparison with the excitation relaxation processes in bulk silica (SiO_2), a detailed mechanism of excitation transfer from solid substrates to adsorbates is revealed for the first time. Another motivation for this work is to draw a comparison between organic and inorganic solids. In our recent studies, energy transfer from polymer hosts to guest dopants in polymeric solids has been shown to occur via ionic processes.[26] It would be interesting to compare and contrast the response of these two materials to high-energy radiation.

Experimental Section

Chemicals. HPLC grade solvents (obtained from Aldrich) such as benzene, pentane, cyclohexane, chloroform, and methanol are used in our experiments. Aromatic probes and quenchers are extensively used throughout this work, including pyrene, biphenyl, *N*,*N*-dimethylaniline, methyl viologen, etc. Probe molecules are adsorbed on solid surfaces from solutions.

Several different types of silicas are used in this work. Granular Davisil silica gel powders with various pore sizes (D60, 60 Å; and D150, 150 Å) were purchased from Aldrich Chemical. These are made from a base-catalyzed hydrolysis and polymerization of silicate acid and used as model systems of porous silicas. The primary particles in Davisils are continuously linked via surface condensation reactions into a rigid three-dimensional network interpenetrated by a multiconnected porous structure. Small amounts of ionic impurities such as Cl^- and SO_4^{2-} present in Davisil silicas are washed out before thermal activation, using distilled and doubly deionized water before use. Pyrogenic aerosil powders with different particle sizes are obtained from Cabot, namely Cab-O-Sil (HS-5, particle size ∼60 Å, surface area ∼ 300 m^2/g; and L-90, particle size ∼300 Å, surface area ∼100 m^2/g). Monospherical silicas with large diameters (M1000, particle size 1000 Å), manufactured by E. Merck, are used together with Cab-O-Sils as the model systems for nonporous silicas. Compared with Davisils, these pyrogenic silicas made by burning $SiCl_4$ in an oxygen−hydrogen flame have the highest purity with a very low content of metal cations and other anions. The nanometer particles of Cab-O-Sils spontaneously adhere together via hydrogen bonding into a loose aggregation, while no such agglomeration is present in large monospherical particles.

Sample Preparation. Silicas exposed to air exhibit surfaces that are covered by physically adsorbed water. Heat treatment of silica powders in a 150 °C oven overnight removes most of the physisorbed water and results in a fully hydroxylated surface with vicinal hydroxyl groups interacting with each other via hydrogen bonding. Further heat treatment at higher temperatures starts to remove chemisorbed water by a condensation reaction. Fourier transform infrared (FTIR) spectroscopy shows that heating to 600 °C removes most of the hydrogen-bonded hydroxyls, and the surface is left with isolated hydroxyls. The surface coverage of hydroxyl groups is ∼5 OH/nm^2 in 150 °C dried silicas, and it is reduced to ∼1.2 OH/nm^2 on 600 °C dried surfaces.[27] Heating at temperatures above 600 °C is of little chemical interest and is not included in our experiments.

Organic probe molecules such as pyrene are adsorbed onto surfaces of thermally activated silicas from alkane solutions. This occurs via hydrogen-bonding interactions between the surface silanol groups and the pyrene. The surface coverage by a specific organic compound is derived from the measurement of its adsorption isotherm. Analysis using the Langmuir adsorption equation[28] shows that the number of adsorption sites for pyrene is greatly reduced on changing the pretreatment temperature from 150 to 600 °C. For the purpose of transient measurements in the diffuse transmittance mode, samples are handled in several different ways in this work, including powder, self-supported disc, and index-matched slurry. Powder samples are used for most of the experiments with silica gel due to its relatively lower scattering power. Loading the solution with probe molecules and transferring the sample to an irradiation cell are carried out under the protection of anhydrous solvents such as pentane and cyclohexane to prevent readsorption of water. Silica powder is further dried in the cell at room temperature under a vacuum of $\sim 10^{-3}$ Torr for ∼3 h. In some cases, when solution loading is not efficient (for example, *N*,*N*-dimethylaniline), powder samples are transferred into the irradiation cell in contact with air, after probe molecules are completely dried onto the silica surface from solution. No difference between these two methods is observed in fluorescence spectroscopy or radiation chemical studies, which is presumably due to the slow process of surface rehydration. For pyrogenic silicas with a high scattering power, thin disc samples (0.1∼0.2 mm thick) are prepared by pressing the vacuum-dried silica powder, followed by rapid transfer into an irradiation chamber connected with a vacuum line. Pressed disc samples are also used for silica gel in low-temperature studies. Index-matched silica gel/cyclohexane slurry systems are used for fast kinetic measurements and spectroscopic studies of the solid−liquid interface.

Pulse Radiolysis. A short pulse of fast electrons (∼0.4 MeV) from a Febetron 706 is used for high-energy radiolysis experiments. The pulse width is ∼2 ns with an energy of ∼200 krad per pulse. Irradiation of opaque silica samples are carried out in three different ways with transient absorption measurements made in the diffuse transmittance mode.

(1) Self-supported silica discs are irradiated in a vacuum-proof metal chamber. After penetrating a thin titanium window into the chamber, the electron beam excites a solid sample at the front surface. Transient intermediates are analyzed by a beam of white light passing through the sample in a cross configuration. In most of the studies, the chamber is evacuated to 1×10^{-3} Torr to avoid oxygen effects. Vapors of organic quenchers and scavengers are introduced into the chamber through the vacuum line. A heating device and a thermal couple are integrated into the sample holder for necessary thermal treatment and activation studies.

(2) A different sample holder is built with a hollow metal block which serves as a liquid nitrogen reservoir is used for

low-temperature measurements.[29] Heat transfer is minimized by keeping a vacuum inside the chamber. The reservoir, when filled with liquid nitrogen, cools a sample on a cold finger in contact with the sample holder down to 100 K. The same cross-excitation-and-probing geometry is applied in transient detection. Measurements at intermediate temperatures are taken by slow warming of the sample holder. The sample temperature is monitored by a thermal couple attached to the sample holder.

(3) Experiments on liquid solutions and solid powders are performed inside a quartz cell with a beam window made of a thin film (~40 μm) of polyethylene terephthalate (PET). The very weak absorbing transient produced in PET film gives a wide spectral window in the visible range (350~700 nm). The loss of the electron beam on the film window is less than 10%. The excellent properties of PET against water and oxygen penetration allows vacuum pumping to 10^{-3} Torr.[20] For diffuse transmittance studies, 1 mm thin cells are used for irradiation of silica powders.

The response of the pulse radiolysis system and the normalization technique used in spectral measurements has been described in our previous publications.[23,26] The absolute yields of transient species produced in irradiated silica are measured in *G* values as conventionally defined, i.e. the number of transient species generated per 100 eV energy loss in *G* values. Transient absorbance of the hydrated electrons produced in a 2 mm water cell (with 0.1 M ethanol and 0.01 M NaOH as scavengers) is used as a relative standard to calibrate the irradiation dosage delivered by the febetron. The absorbance of a silica sample measured at a specific wavelength right after the pulse under the identical irradiation conditions is used for the calculation of the *G* value of a transient species.[26]

Diffuse Transmittance and Reflectance. Absorption spectra of silica samples are taken in diffuse reflectance and transmittance modes on a Cary UV-visible spectrometer equipped with an integrating sphere attachment. Applicability of the Lambert−Beer approach to the diffuse transmittance is examined by making measurements on 1 mm thick D60 powder samples loaded with a known amount of perylene. Such experiments show that transmittance is more sensitive than reflectance and it exhibits a linear relation against the probe concentration at low loadings. However, spectra with absorbances larger than 0.3 suffer a nonlinear distortion, and the Lambert−Beer approach is no longer valid.[31] This is particularly important for the transient absorption measurements on powder and disc samples in pulsed experiments.

FTIR Spectroscopy. Surface structures of silicas and adsorption of organic molecules are examined with FTIR spectroscopy using a Mattson Instruments' Galaxy-5000 FTIR spectrophotometer. It consists of a cube-corner interferometer with a KBr beam splitter, a He−Ne laser quadrature as the internal standard, and a DTGS detector which covers the mid-IR range from 400 to 5000 cm^{-1}. A microprocessor is integrated in the spectrometer to carry out the fast Fourier transform of acquired interferograms. WinFirst software (Mattson Instruments) is installed in an IBM-compatible personal computer with a DX-486 processor to control the spectrometer settings and data handling in a Microsoft Window environment. Normally, spectra are taken in the transmission mode over 16 or 32 scans with a resolution of 4 cm^{-1}. Measurements of silica samples are made on pressed thin discs in a homemade infrared cell with a pair of CaF_2 windows. This allows in situ heat treatment in vacuum and adsorption of organic molecules from the gas phase.

Fluorescence Spectroscopy. Both steady-state and time-resolved fluorescence spectroscopy is used to examine the polarity of the surface environment and the possible aggregation of probe molecules on silica surfaces. Steady-state fluorescence spectra are taken on a SLM-5000C spectrofluorometer. The fluorescence lifetime of pyrene on silica is measured by using a PRA nitrogen laser (0.13 ns pulse width) as the excitation source and a Hamamatsu microchannel plate PMT (R1644U) as the detector. Pyrene excimer emission is observed on 150 °C dried D60 with pyrene loading above 1.0×10^{-5} mol/g and on 600 °C dried D60 with pyrene loading above 1.5×10^{-6} mol/g. Aggregation of pyrene well below the monolayer coverage of the available silica surface is indicative of a nonhomogeneous distribution of pyrene due to a limited number of adsorption sites.

γ-Radiolysis and Product Measurements. γ-Irradiation of silica samples is carried out in sealed quartz tubes by exposure to a ^{60}Co source for 30 min. The dose rate is measured by the Fricke dosimeter to be ~24 rad/s. Electron paramagnetic resonance (EPR) spectra are recorded on a Varian EPR spectrometer (E-lines century series) equipped with an X-band klystron and a TE_{102} type cavity, operating at ~9.5 GHz and with 100 MHz magnetic modulation. The *G* value is determined by comparison with diphenylpicrylhydrazyl (DPPH).[32] Steady-state irradiation and EPR measurements of silica samples are made at liquid nitrogen temperature under vacuum, after thermal activation and probe loading. Samples are also irradiated at room temperature, and evolution of hydrogen gas is measured using a gas chromatograph (Carle) with a thermoconductivity detector and a packed column (80% PPN and 20% PPΦ). The instrument is calibrated by measuring a series of hydrogen gas samples of known quantities.

Results and Discussion

1. Irradiation of Blank Silicas. *Hydrogen Production.* Steady-state EPR measurements of γ-irradiated silica samples (T_a = 140 °C) at 77 K clearly show the double-line spectrum of hydrogen atoms with the characteristic hyperfine splitting a = 508 G and g = 2.0036. This is in agreement with the early work.[8,9] The central part of the EPR spectrum consists of overlapping signals from radiation-produced defect centers. Further studies of defect creation in high surface area silica in comparison with bulk silica will be addressed elsewhere. In a series of irradiated D60 powder samples pretreated at different temperatures above 150 °C, the same hydrogen EPR spectrum is observed with decreasing signal intensity, which also agrees with the previous reports.[8] Two possible mechanisms have been

$$\equiv\text{SiOH} \xrightarrow{h\nu} \equiv\text{SiO}^{\bullet} + \text{H} \quad (1)$$

$$e^- + \equiv\text{SiOH} \rightarrow \equiv\text{SiO}^- + \text{H} \quad (2)$$

proposed for hydrogen production in irradiated silica, namely, radiolytic homolysis of the O−H bond of hydroxyl impurities in silica[33] and dissociative electron attachment to silanol groups.[34] Observation of the nonbridging oxygen hole centers (≡$SiO^{\bullet}$) by EPR spectroscopy suggests that homolysis is the major process.[33] Photoionization experiments were carried out to test reaction 2. Electrons are ejected into silica from aromatic adsorbates such as pyrene via a resonant two-photon absorption, leaving long-lived radical cations on the surface. No EPR signal from hydrogen atoms is detected at 77 K,[35] which does not favor dissociative electron attachment. It will be shown later that H atoms are produced in reaction 1 via an excitonic process.

Gas chromatography measurements found that γ-irradiation at room temperature of D60 powder dried at 140 °C produces copious amounts of hydrogen gas. The yield of H_2 gas is

measured to be $G(H_2) = 1.6$ with the dosage corrected by the density and the mass absorption coefficient of the silica powder. Dimerization of the hydrogen atoms initially produced is suggested for the production of molecular hydrogen in irradiated silicas.[36]

$$H + H \rightarrow H_2 \quad (3)$$

The results of the effect of organic adsorbates on the production of H_2 gas will be given later in this paper. Evolution of H_2 in the form of gas bubbles is also observed in irradiated silica slurries in alkanes and alcohols with silica activated at different temperatures. This is in agreement with the early work by Allen.[2]

Surface-Trapped Charges. Time-resolved measurements after the 2 ns electron pulse revealed a short-lived transient in silica gel D60 ($T_a = 140$ °C), that exhibits a broad absorption spectrum in the visible region with its maximum around 600 nm (Figure 1a). The decay of this transient is nonexponential with a half-life of ~50 ns (insert of Figure 1a). Typical electron scavengers such as oxygen, nitrous oxide, and chloroform introduced through the gas phase quench the transient band mainly in a static fashion. This indicates that it is a surface species derived from electron trapping. The assignment of this new species to a surface-trapped electron (e_{tr}^-) is supported by photoionization of pyrene in D60 ($T_a = 140$ °C) where electrons are ejected and trapped on the silica surface, giving rise to the same absorption band around 600 nm.[37] In comparison with the diffusion-controlled oxygen quenching of radical anions such as $Py^{-\bullet}$ and solvated electrons e_s^- in the liquid phase, the slight dynamic quenching of e_{tr}^- by O_2 might result from a slow intrinsic rate on the silica surface due to a lack of solvation and the cage effect. The increasing absorption in the deep-UV part of the spectrum might be due to the overlapping bands of the E' centers ($\equiv Si^{\bullet}$) and $\equiv SiO^{\bullet}$.[38]

Measurements are also made in an electron beam irradiated D60/cyclohexane slurry. The same absorption band is observed with a half-life of ~30 ns, and again it is statically removed by addition of chloroform to the slurry. Modification of the silica surface induces a variation in the lifetime of the trapped electron e_{tr}^-, in agreement with its assignment to a surface species. Longer lifetimes were observed in Na^+ exchanged D60, and D60 with triethylamine adsorbed on the surface. Meanwhile a shorter lifetime was observed on D60 with physisorbed water. When pulse radiolysis and spectral measurements are carried out in the low-temperature Dewar, the surface-trapped electrons exhibit considerably longer lifetimes which increase with decreasing sample temperature, e.g. $t_{1/2} = 4 \sim 5$ μs in D60 at 150 K. Oxygen quenching of the surface-trapped electrons at 150 K exhibits a purely static pattern due to significant oxygen adsorption on the silica surface at this temperature (Figure 1b).[39]

Recently, Mao and Thomas have observed, during a post-irradiation annealing, a strong thermal luminescence of pyrene from pyrene-loaded silica gel samples irradiated in a photo reactor at 77 K. Geminate ion recombination between pyrene radical cations and silica-trapped electrons is suggested for the production of pyrene singlet and triplet excited states (S_1 and T_1).[40] Direct observation of the surface-trapped electrons in pulse radiolysis confirms the concepts of electron trapping and subsequent recombination on the silica surface. The same species is also observed in other porous silica gels and in nonporous silicas such as Cab-O-Sils and M1000. Figure 1c shows the temperature effect on the decay of the surface-trapped electron in a M1000 disc ($T_a = 140$ °C) under vacuum. Decreasing temperature gives rise to an increased lifetime of e_{tr}^-. The same static quenching by O_2 and N_2O is observed in such a large particle silica as that in silica gel D60, again indicating that it is produced on the surface rather than in the bulk.

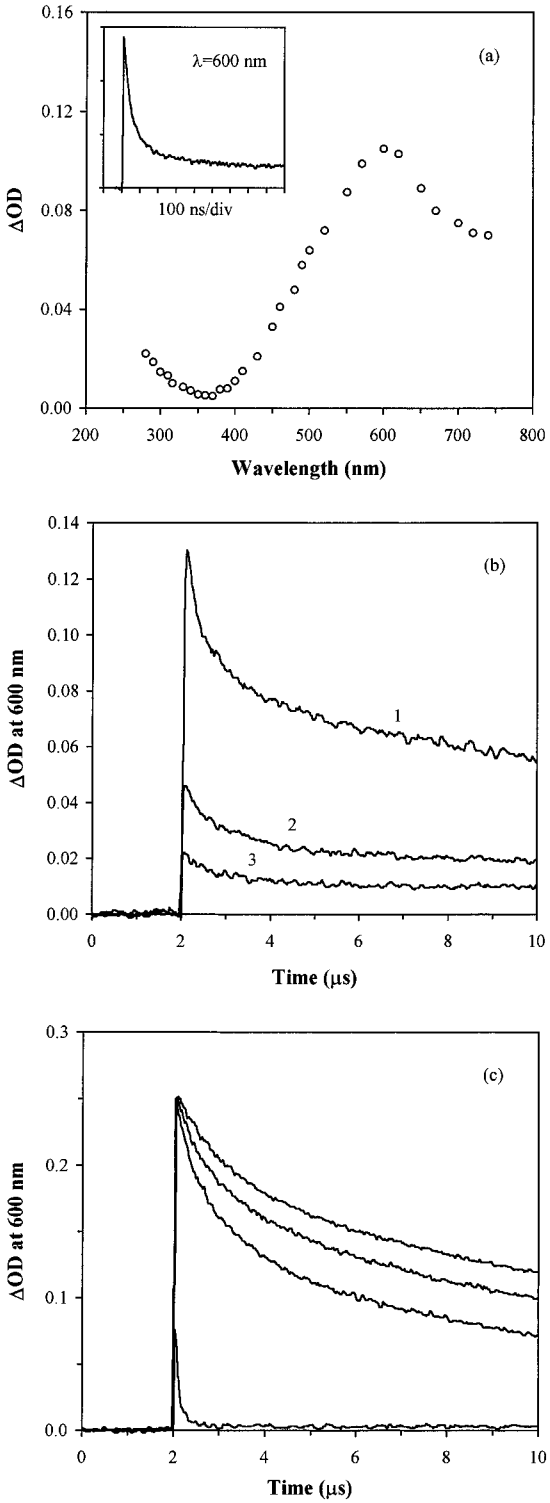

Figure 1. (a) Transient absorption spectrum of trapped electrons on the silica gel D60 surface ($T_a = 140$ °C), taken at the end of the pulse (~7 ns). Inset shows the time-resolved decay trace monitored at 600 nm. (b) Oxygen quenching of surface-trapped electrons in silica D60 ($T_a = 140$ °C) measured at 150 K. Oxygen pressures are (1) 0 Torr; (2) 45 Torr; (3) 90 Torr. (c) Temperature effect on the decay of surface-trapped electrons in monospherical silica M1000 under vacuum. $T =$ 150, 180, 220, and 298 K from the top trace to the bottom.

Dehydroxylation of D60 at 600 °C removes the surface-trapped electrons produced on irradiation and gives rise to a new broad absorption band centered at 550 nm (Figure 2). The

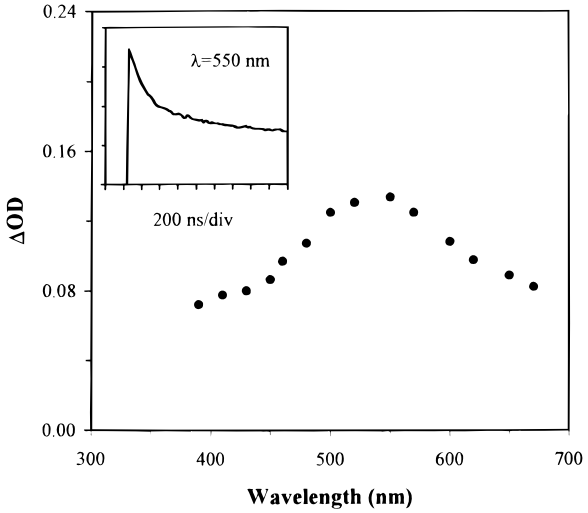

Figure 2. Transient absorption spectrum of surface-trapped holes in blank D60 (T_a = 600 °C). Inset shows the decay trace monitored at 550 nm.

new band is relatively long-lived (inset of Figure 2), and it is not quenched by typical electron scavengers such as oxygen, N_2O, and chloroform. However, adsorption of cyclohexane statically decreases the yield of this new transient, and it is completely removed in a D60/cyclohexane slurry. At this stage, the species is tentatively assigned to a trapped hole on the dehydroxylated surface, but its structure is not clear. Early steady-state studies have observed that dehydroxylated silica turns blue after γ-irradiation. These surface color centers were found to be acidic and responsible for the subsequent carbonium ion formation and dealkylation of isopropylbenzene.[11,12] It confirms our assignment of the 550 nm transient band to surface-trapped hole centers. The removal of the surface-trapped electron by dehydroxylation suggests that the electron might be trapped by the hydrogen-bonded surface silanol clusters, but not by the isolated hydroxyls. In comparison with bulk silica, production of these surface-trapped charges is indicative of an enhanced charge trapping and ionic reactions by the surface.

2. Irradiation of Silicas Loaded with Pyrene. *1-Hydropyrenyl Radicals on the Silica Surface.* Due to its well-established chemical reactions and excellent spectroscopic properties, pyrene is used to examine the radiation chemistry on silica surfaces. Irradiation of a 1.8×10^{-6} mol/g pyrene-loaded D60 sample (T_a = 140 °C) produces a new transient spectrum different from that of the blank silica. The surface-trapped electron is little affected at this level of pyrene loading and thus contributes a very short-lived spectral component around 600 nm. The spectrum taken at ~0.5 μs after the decay of the surface-trapped electron clearly shows the production of pyrene transient species (Figure 3a). The absorption peak around 450 nm is identified as the pyrene cation radical, which is also supported by spectroscopic measurements at low temperatures (see Figure 7c). The weak band at 490 nm is only slightly affected by oxygen, indicating that a major portion of the absorption might be due to the cation spectrum. Contrary to the radiolysis of pyrene in organic liquids and polymers, the yield of the pyrene anion produced on the silica surface is very low. The absorption band around 400 nm has the highest intensity and is assigned to the 1-hydropyrenyl radical (PyH•). This is based on the spectral shape and the mechanistic studies described in the following part of this work. The transient absorption spectrum of PyH• produced via the hydrogen addition reaction in acidic methanol is also shown in Figure 3a for comparison.[25]

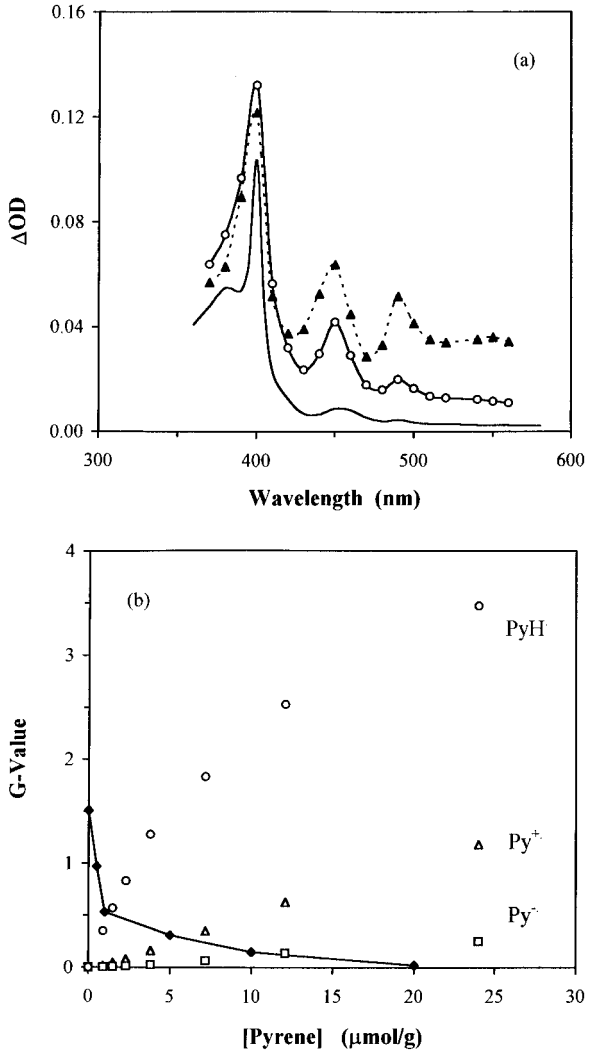

Figure 3. (a) Transient absorption spectra of the irradiated Py/D60 powder sample (circles, T_a = 140 °C, and triangles, T_a = 600 °C), taken at 0.5 μs after the pulse in vacuum. The pyrene loading is [Py] = 1.3×10^{-6} mol/g. The smooth line gives the absorption spectrum of 1-hydroxylpyrene radicals produced in acidic MeOH with [Py] = 0.010 M. (b) G values of pyrene transient species produced on the surface of D60 (T_a = 140 °C) in electron beam irradiation. The yields of hydrogen gas produced in γ-irradiated D60 (T_a = 140 °C) are also shown for different pyrene loadings (connected points).

G values of these transients are measured in D60 samples with different pyrene loadings (Figure 3b). The yield of PyH• increases almost linearly with the increasing pyrene coverage and shows some saturation at pyrene loadings larger than 10^{-5} mol/g. This is due to pyrene aggregation as shown by the static excimer formation in fluorescence spectroscopy. The G value of PyH• production at the highest loading [Py] = 2.45×10^{-5} mol/g is measured to be G(PyH•) = 3.6, while the yield of the pyrene cation is $G(Py^{+\bullet}) = 1.2$ and that of the pyrene anion is $G(Py^{-\bullet}) < 0.1$.

$$h^+(SiO_2) + Py \rightarrow Py^{+\bullet} \quad (4)$$

$$e^-(\text{conduction band}) + Py \rightarrow Py^{-\bullet} \quad (5)$$

The low yield of the pyrene anion is consistent with the minimal effect of pyrene loading on the surface-trapped electron.

Figure 3b also shows that the H_2 gas yield decreases with increasing pyrene loading. A comparison between the steady-state measurements of the reduction in H_2 gas yield and the

time-resolved measurements of the simultaneous production of PyH• radicals at different pyrene coverage indicates that hydrogen atoms might be the precursor of PyH•. The discrepancy between the decrease of the H_2 yield and the corresponding increase of the PyH• yield may be settled by considering that the PyH• yields are measured at 0.5 μs after the excitation pulse without including the contribution from the slow component of PyH• formation (see Figure 4a). The difference in dose rates between pulse and steady-state radiolysis might be another factor that affects the recombination rate of H atoms. The low dose rate in γ irradiation favors the H addition reaction over dimerization in the steady-state measurements.

Formation of 1-Hydropyrenyl Radicals: Mechanism and Kinetics. The above measurements of the transient species produced on irradiated silica surfaces shows that the major process is the formation of the PyH• radical. Previous work in liquid solutions has suggested that the PyH• radical can be produced from two different reaction mechanisms, i.e. hydrogen addition to pyrene and protonation of the pyrene anion radical.[25,41,42]

$$H + Py \rightarrow PyH^{\bullet} \quad (6)$$

$$H^{+} + Py^{-\bullet} \rightarrow PyH^{\bullet} \quad (7)$$

Both mechanisms seem possible on silica surfaces. For reaction 6, hydrogen atoms are produced in reaction 1 at a very early stage when excitation energy is transferred to the surface hydroxyls (≡SiOH) and produces hydrogen atoms. Alternatively, charge separation of an electron-hole pair might result from electron scavenging by pyrene and hole trapping at the nonbridging oxygen hole centers (NBOHC) with the release of a proton H^+.[43]

$$h^{+}(SiO_2) + \equiv SiOH \rightarrow \equiv SiO^{\bullet} + H^{+} \quad (8)$$

Subsequent ion recombination reaction 7 on the silica surface leads to the formation of PyH• as in alcohol solutions.[41] These two different processes also show one common feature, i.e. they are surface hydroxyl controlled reactions. The following experimental results, particularly the scavenging effect by foreign gases and organic vapors, give favorable evidence for the hydrogen addition reaction. Protonation of the pyrene anion as depicted by reaction 7 is an insignificant process on silica surfaces.

Time-resolved measurements of PyH• formation kinetics at 400 nm on D60 samples with different pyrene loadings revealed a distinct two-component growth pattern with a fast component which rises with the excitation pulse and a slow part extending over many microseconds (Figure 4a). The slow formation of PyH• over 20 μs exhibits its largest amplitude around a pyrene loading of 8 μmol/g. The introduction of 2 mbar of oxygen removes the slow growth, leaving the fast component unaffected. However, nonporous Cab-O-Sil HS-5 samples (T_a = 140 °C) only show the fast formation of PyH• without the slow component on the microsecond time scale. Nanosecond measurements on semitransparent HS-5 disc samples with different pyrene loadings found that the PyH• formation kinetics is quite nonexponential, with ~70% of the radical formed within the system response of ~7 ns and the other 30% formed over ~100 ns (Figure 4b). No slow growth is observed after 300 ns, which is different from that observed in silica gel D60. It is also found that the kinetics of PyH• formation is independent of pyrene loadings in Cab-O-Sil. The effect of oxygen on the PyH• radical formation kinetics is also shown in Figure 4b. The PyH• growth

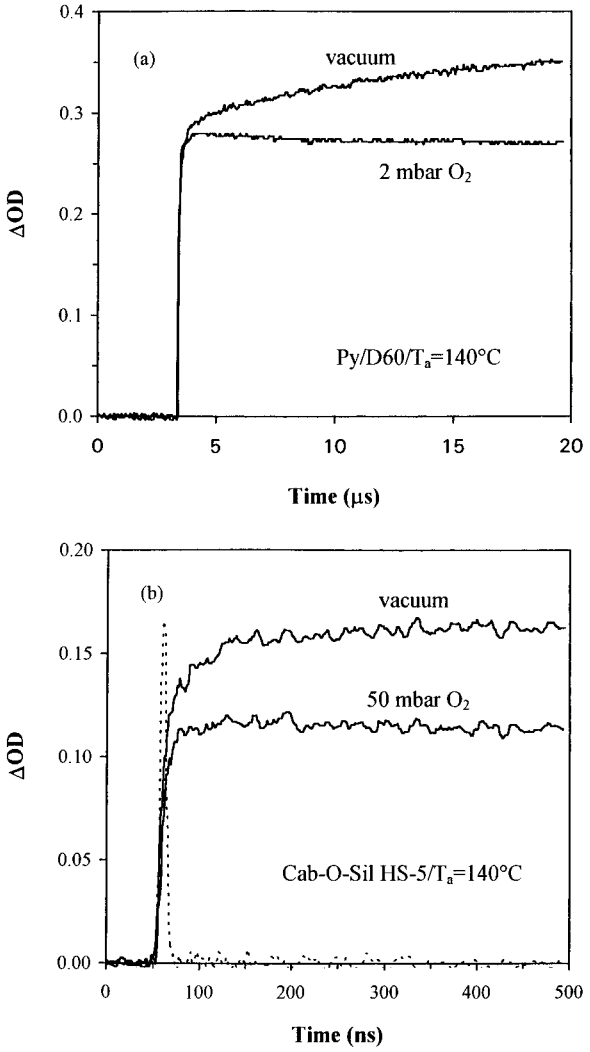

Figure 4. (a) Time-resolved kinetic trace of PyH• formation in silica gel D60 (T_a = 140 °C), monitored at 400 nm in vacuum and under 2 mbar of oxygen. [Py] = 5.0×10^{-6} mol/g. (b) PyH• formation kinetics in a Cab-O-Sil HS-5 disc sample (T_a = 140 °C) in vacuum and under 50 mbar of oxygen. The pyrene loading is 2.0×10^{-6} mol/g. The pulse response of the measurement system is shown in a dashed line.

that is slower than ~5 ns (after the deduction of the instrument response) is removed by 50 mbar oxygen, indicating that oxygen reacts with the precursor of hydropyrenyl radicals.

Effect of Foreign Gases. Figure 5 shows the effect of foreign gases on the yield of the PyH• radical produced in 140 °C dried D60. With increasing oxygen pressure the fast component is statically quenched, and the pressure at a 50% reduction of PyH• is around 160 mbar. In contrast to oxygen quenching, nitrous oxide gradually suppresses the slow growth of PyH• and shows no quenching of the fast component. The comparable oxidation reactivities of oxygen and nitrous oxide (as we have observed for the surface-trapped electrons) and the dramatic difference in static quenching of the PyH• radical clearly indicate that they are not reacting with any negatively charged precursor, neither the surface-trapped electron nor the pyrene anion radical. The above experiments suggest that the PyH• radical is formed on hydroxylated silica surfaces via a hydrogen addition reaction. Actually, the mechanisms of the reactions of O_2 and N_2O with hydrogen atoms are quite different. This results in the distinct static quenching patterns. The reaction between O_2 and H is predominated by a three-body process in the liquid phase and also on silica surfaces, while that between N_2O and H is simply a bimolecular reaction.

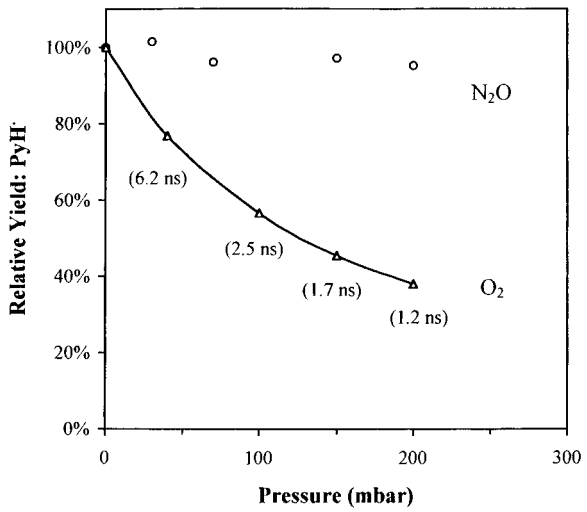

Figure 5. Quenching effect of foreign gases on the yield of PyH• produced in D60 (T_a = 140 °C). [Py] = 2.0 × 10^{-6} mol/g. The estimated lifetimes of H atoms are labeled at different oxygen pressures.

$$H + O_2 + M \rightarrow HOO^{\bullet} \quad (9)$$

$$H + N_2O \rightarrow N_2 + OH^{\bullet} \quad (10)$$

In the gas phase, reaction 9 is collision controlled with a negative activation energy,[44] while reaction 10 has an activation energy as high as 16.6 kcal/mol and a rate constant of 2.1 × 10^6 M^{-1} s^{-1} even at 773 K.[45] In aqueous solution, the rate constant for reaction 9 is ∼3.0 × 10^{10} M^{-1} s^{-1}, which is much larger than the rate constant of 2.1 × 10^6 M^{-1} s^{-1} for the reaction N_2O + H.[46] The efficient static quenching of PyH• by oxygen in silica systems is due to reaction 9 where the silica surfaces serve as the third body M. From the above nanosecond time-resolved measurements on Cab-O-Sil (Figure 4b), the rate constant of reaction 9 is estimated to be 4.0 × 10^6 $mbar^{-1}$ s^{-1} or 5.6 × 10^6 $Torr^{-1}$ s^{-1}. Therefore, at an oxygen pressure of 160 mbar, the lifetime of H atoms is ∼1.6 ns, which implies from Figure 5 that about 50% of the PyH• radicals are formed within ∼1.6 ns. The much slower rate of reaction 10 results in little quenching of the fast formation of the H−pyrene adduct over the pressure range used in the experiments.

On the basis of the above kinetic studies and gas quenching effects, we attribute the fast formation of PyH• to the H + Py reaction at the same site within the same pore where a H atom is produced in the vincinity of pyrene. The slow formation in porous silica gel over many microseconds is attributed to the addition reaction between H atoms and pyrene in separate pores. This interpore reaction is absent in nonporous Cab-O-Sil samples, indicating that H atoms, like small gas molecules, are not extensively adsorbed on the silica surface. The large mesopore volume in Cab-O-Sil due to the loose aggregation of the silica particles favors the escape of H atoms. In contrast, confinement of H atoms by the multiconnected network of nanometer size pores in silica gel gives rise to the interpore reaction. The rate of this reaction is limited by the gaslike diffusion of H atoms within the porous structure to find pyrene before recombination with another H atom or escape from the silica granule into vacuum. It is necessary to point out that the *G* values of the PyH• radical in D60 samples are only measured for the fast intrapore component (Figure 3b), since it is difficult to completely capture the PyH• signal from the slow interpore reaction over tens of microseconds due to the simultaneous decay of the PyH• radical on the surface.

Scavenging Effects. Cyclohexane and chloroform vapor may be coadsorbed to pyrene-loaded D60 samples (T_a = 140 °C).

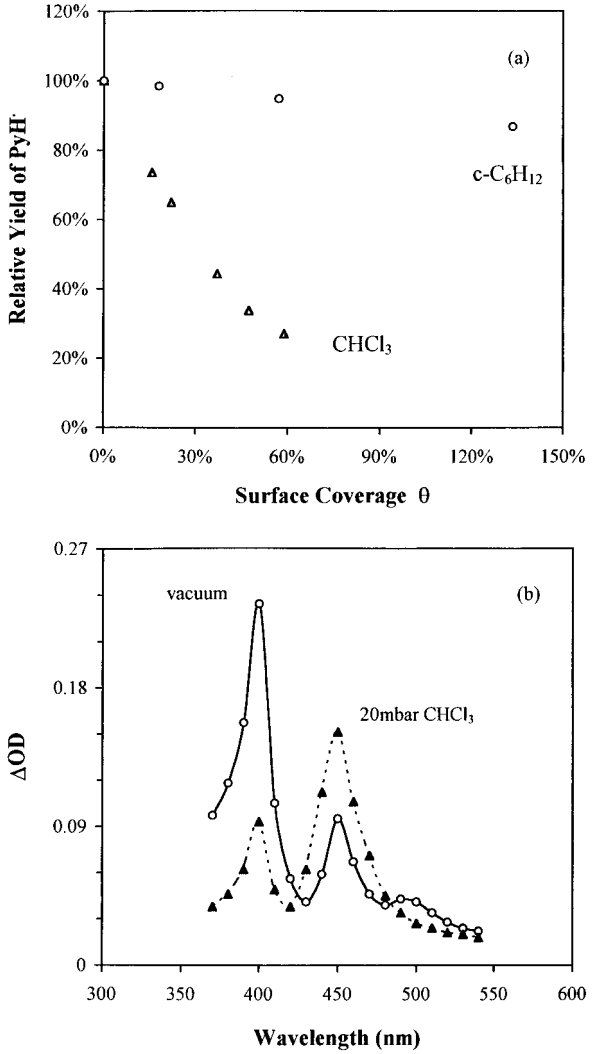

Figure 6. (a) Static quenching of PyH• derived from the intrapore H-addition reaction by cyclohexane and chloroform at different surface coverages. (b) Spectral variation indicative of an increased production of pyrene cation radicals with the quenching of PyH• by introduction of 20 mbar of $CHCl_3$. [Py] = 1.3 × 10^{-6} mol/g.

Figure 6a shows the static quenching of PyH• by cyclohexane and chloroform at different surface coverages. Cyclohexane is known to react with hydrogen atoms with a rate constant of 7.8 × 10^7 M^{-1} s^{-1} in the liquid phase.[46]

$$H + c\text{-}C_6H_{12} \rightarrow H_2 + c\text{-}C_6H_{11}^{\bullet} \quad (11)$$

Due to the formation of molecular hydrogen in the above reaction, evolution of hydrogen gas bubbles is readily observed in electron beam irradiation of D60/cyclohexane slurry systems with silica dried at both 150 and 600 °C.

It is surprising to find that even at a monolayer coverage by c-C_6H_{12}, 90% of the PyH• radicals are still unscavenged. This cannot be understood by the Stern−Volmer kinetics of the competing homogeneous reactions as conventionally observed in liquid solutions. At a surface coverage that is lower than 10%, cyclohexane scavenges H atoms for the interpore H + Py reaction and removes the slow formation of PyH•. However, for the very inhomogeneous H addition reaction between the tightly confined H atom and pyrene, a monolayer spread of cyclohexane does not compete efficiently for the H atom, simply because the reaction rate for H + Py is nearly 2 orders of magnitude faster than that of c-C_6H_{12}. In fact, PyH• radicals are readily observed on pyrene-loaded D60 samples (T_a = 140

°C) in a cyclohexane index matched slurry where the lifetime of the H atoms is 1∼2 ns. This agrees with nanosecond absorption measurements showing that the rise of the PyH• signal is within the system response (∼7 ns). After a correction for the dose absorbed by cyclohexane in the pore volume, the yield of PyH• is about 25% of that observed in a dry powder sample with the same loading of pyrene. If the lifetime of the H atoms is taken as ∼1 ns due to the scavenging reaction 11 in the silica pores filled with cyclohexane, then from a Stern−Volmer approach of homogeneous reactions less than 2% of the hydrogen atoms should be converted to PyH•. It is thus concluded that the significant yield of the PyH• radicals produced within 1∼2 ns is derived from the inhomogeneous intrapore H + Py reaction on the silica surface.

Additional evidence for the inhomogeneous addition reaction comes from the PyH• yield measurements as shown in Figure 3b. At a pyrene loading of 2.45×10^{-5} mol/g, which corresponds to a surface coverage of about 6%, the G value of PyH• ($G_{PyH•} = 3.6$) produced from the intrapore reaction accounts for 85% of the total yield of the hydrogen atoms $G_H = 4.2$ (as will be given later). This strongly suggests that hydrogen atoms are not produced randomly at any surface hydroxyl sites but rather at those which are responsible for pyrene adsorption.

A similar abstraction reaction is expected to occur for $CHCl_3$, with a rate constant of 1.1×10^7 M^{-1} s^{-1}, which is slower than that of reaction 11.[46]

$$H + CHCl_3 \rightarrow H_2 + {}^{\bullet}CCl_3 \text{ or } HCl + {}^{\bullet}CHCl_2 \quad (12)$$

However, $CHCl_3$ exhibits a much more efficient static quenching of PyH• than cyclohexane. This indicates that the two scavengers are not reacting with the same precursor, i.e. the hydrogen atom. The concomitant increase of the pyrene cation radical yield with the static quenching of PyH• by $CHCl_3$ suggests that chloroform reacts with the electrons in the conduction band. Figure 6b illustrates the increased production of pyrene cation radicals with the quenching of PyH• radicals by coadsorbed $CHCl_3$ on the D60 surface ($T_a = 140$ °C).

$$e^-(\text{conduction band}) + CHCl_3 \rightarrow CHCl_2^{\bullet} + Cl^- \quad (13)$$

The same has been observed in solid polymers, where positive charge transfer to pyrene is enhanced at the expense of the static quenching of pyrene excited states by $CHCl_3$.[26] As will be shown later, the electron scavenging reaction 13 prevents the exciton from being localized at the hydroxyl sites, and therefore reduces the production of hydrogen atoms on the silica surface. Such an electron scavenging effect is also observed in silica gel D60 with different amounts of Cd^{2+} ion exchanged onto the silica surface. Again PyH• is statically quenched, and the released positive hole reacts with pyrene, leading to increased production of pyrene radical cations.

Temperature Effect. The yield of the prompt formation of PyH• from the intrapore reaction on the 140 °C dried D60 surface exhibits a strong temperature dependence as shown in Figure 7a. Time-resolved kinetic traces at 400 nm show that the amplitude of the fast component measured right after the pulse is gradually reduced with decreasing temperature and the slow component of the PyH• formation from the interpore reaction is absent below 250 K. Since the intrapore reaction between a H atom and pyrene at the same site does not involve extensive diffusion, the decrease in the prompt PyH• production was attributed to an activation energy for reaction 6, as found for the other H addition reactions with aromatic compounds.[47,48] If the rate for H atoms to escape the intrapore reaction (denoted as k_s) is treated as a weak function of temperature, and the rate of the addition reaction is expressed in the Arrhenius form $k_r = k_0 \exp(-E_a/RT)$, the yield of PyH• can be approximately related to temperature by the following equation

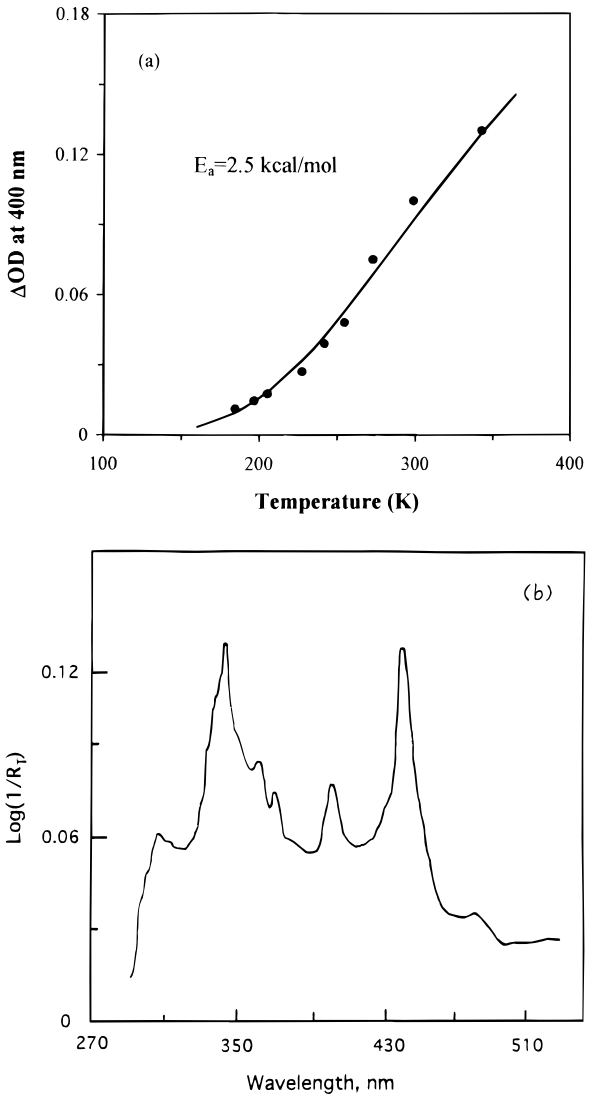

Figure 7. (a) Temperature effect on the intrapore yield of PyH• produced on the D60 surface ($T_a = 140$ °C) in vacuum. [Py] = 2.0×10^{-6} mol/g. The solid line gives the Arrhenius fit of the experimental data with an activation energy of $E_a = 2.5$ kcal/mol. (b) Diffuse reflectance absorption spectrum of a γ-irradiated Py/D60 ($T_a = 140$ °C) powder sample taken at 77 K. [Py] = 4.5×10^{-6} mol/g.

$$\frac{Y_\infty}{Y} - 1 = \frac{k_s}{k_0}\exp\left(\frac{E_a}{RT}\right) \quad (14)$$

where Y and Y_∞ are the yields of PyH• measured in OD at temperature T and extrapolated to the high-temperature limit, respectively. Different Y_∞ are tried for the optimal linear regression of the $\ln(Y_\infty/Y - 1) \sim 1/T$ data. The best fitting of the data points in Figure 7a using $Y_\infty = 0.28$ gives an activation energy $E_a = 2.5$ kcal/mol, which compares well with those of benzene and toluene.[47] The significantly larger Y_∞ than the PyH• yield measured at room temperature indicates that a certain percentage of hydrogen atoms escape the intrapore addition reaction.

As a result of the activation-controlled addition reaction, more hydrogen atoms escape from the H + Py reaction at lower temperatures. Steady-state EPR measurements are carried out on γ-irradiated silica samples at 77 K. The double-line EPR

spectrum of H atoms is observed on D60 with different pyrene loadings, and the intensities of the EPR signals are little affected by pyrene. The diffuse reflectance spectrum of a pyrene-loaded D60 sample ([Py] = 4.0×10^{-6} mol/g), which is γ-irradiated at 77 K and then transferred to the low-temperature attachment in the UV−visible absorption spectrometer, shows the presence of a weak PyH$^{\bullet}$ absorption at 400 nm along with a strong $Py^{+\bullet}$ band around 450 nm (Figure 7b). Hardly any signal is observed from the pyrene anion radical. Using the pyrene cation band as the internal reference, the yield of the PyH$^{\bullet}$ radical band is less than ~8% of that observed in time-resolved measurements at room temperature. If we consider the slight annealing during the sample transfer, the percentage number given here only serves as an estimation of the upper limit of the PyH$^{\bullet}$ yield. The above EPR and diffuse reflectance studies of the temperature effect on radiolytic products confirm that the PyH$^{\bullet}$ radical is produced in silica from the activation-controlled hydrogen addition reaction.

Particle Size Effect. Radiation-induced reactions on surfaces of nonporous silica (T_a = 140 °C) of various particle sizes are studied to examine the extent of energy transfer from the bulk SiO_2 to the surface. The H adduct of pyrene is observed on the surfaces of Cab-O-Sil HS-5 (particle size ~ 60 Å) and L-90 (size ~ 300 Å), and monospherical silica M1000 (size ~ 1000 Å). Typical data are illustrated in Figure 4b for HS-5. There are two important observations: (1) there is no interpore H + Py reaction which is different from that to silica gels and (2) H atoms are not adsorbed on the surface, otherwise the H addition reaction across the surface would result in a slow production of PyH$^{\bullet}$. Monospherical silica M1000 is particularly interesting in the particle size comparison. It has a relatively flat surface with no pores that are detectable by a mercury porosimetry. However, helium porosimetry shows that tiny orifices of 4 Å size exist on the surface.[49] Therefore, any chemistry, as probed by pyrene, occurs exclusively on the particle surface. Irradiation of a pyrene-loaded M1000 disc (pretreated at 140 °C) leads to the formation of PyH$^{\bullet}$ and $Py^{+\cdot}$ as shown in Figure 8a. No pyrene anion is produced. The considerably lower yield of pyrene cations is indicative of a less efficient positive charge transfer to pyrene. This is due to a larger average bulk-to-surface separation. In agreement with the above transient measurements, product analysis shows much less oxidative degradation of pyrene on the irradiated M1000 surface. The significant yield of PyH$^{\bullet}$ suggests that transfer of energy initially deposited inside a 1000 Å particle to its surface is quite efficient! Formation of PyH$^{\bullet}$ exhibits a slow growth within 2 μs (figure 8b). The inset of Figure 8a shows a more efficient oxygen quenching with 50% reduction of the PyH$^{\bullet}$ yield at an oxygen pressure of ~60 mbar. This is different from that observed in silicas of small particle structures such as D60 and Cab-O-Sil HS-5. Meanwhile, chloroform exhibits a smaller precursor quenching effect on the formation of the H adduct. The difference between these two types of silicas is derived from the distribution of hydroxyl groups within the different size particles.

Isotopic exchange reaction has been a reliable technique to discriminate the surface ≡SiOH from the internal ≡SiOH in different silica samples.[50,51] The following isotopic exchange reaction of D_2O with silica surfaces is carried out in vacuum with D_2O vapor introduced and HOD product removed through multiple loading−heating−pumping cycles.

$$\equiv SiO-H + D_2O \rightarrow \equiv SiOD + HOD \qquad (15)$$

In situ FTIR studies of samples treated in this way show that more than 90% of the hydroxyl groups in silica gel D60 are present on the surface and can be completely exchanged to ≡SiOD (Figure 9a). However, for M1000, a significant amount of the hydroxyls exist inside the particles and are not subject to the isotopic exchange reaction (Figure 9b). These internal hydroxyls account for about 40% of the total hydroxyl content in M1000. Because of the presence of these hydroxyl impurities in the bulk SiO_2, the energy loss in the bulk silica of M1000 should produce H atoms inside the particles, just like H atoms produced on the surface. The more efficient oxygen quenching is due to an increased separation between H atoms in the bulk and pyrene on the surface. Hydrogen atoms which are diffusing out to the surface are available to both oxygen and pyrene. The smaller electron scavenging effect by chloroform results from the shielding of radiation generated electron−hole pairs inside the large particles. The slow formation of PyH$^{\bullet}$ over a microsecond is attributed to the diffusion process of H atoms inside the particles before their reaction with pyrene on the surface. Kinetic traces of the PyH$^{\bullet}$ radical formation in Cab-O-Sils with smaller particle sizes are also given in Figure 8b for comparison. The increasing proportion of the slow component in the order of increasing particle sizes from HS-5 and L-90 to M1000 is due to the larger contribution from H atoms produced in the bulk. The correlation between the time constants of the slow formation of PyH$^{\bullet}$ and the particle sizes

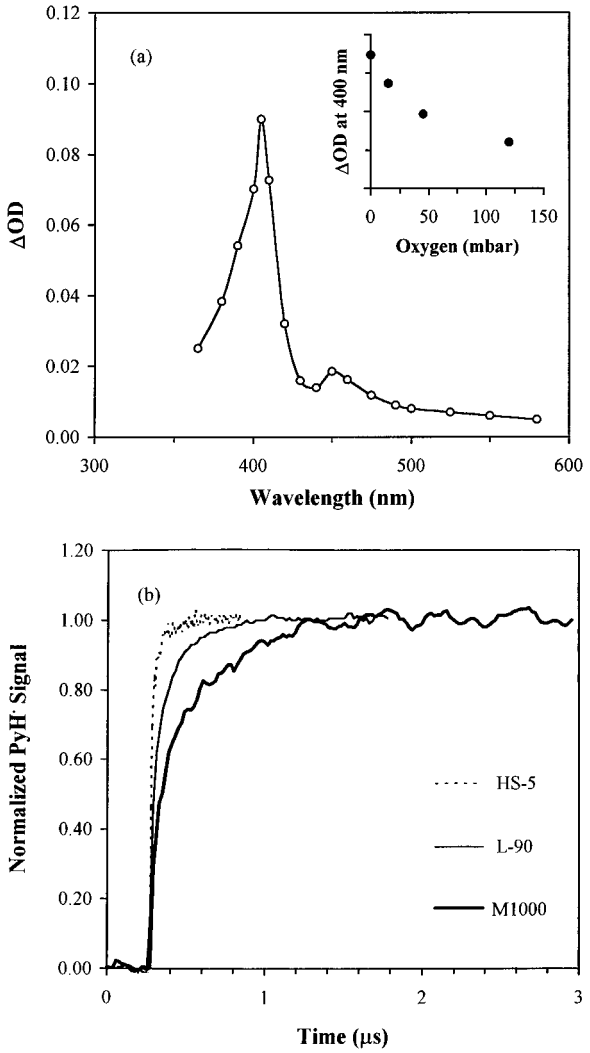

Figure 8. (a) Transient absorption spectrum of an irradiated Py/M1000 disc sample, taken at 0.5 μs after the pulse in vacuum. [Py] = 1.2×10^{-6} mol/g. Inset shows the oxygen quenching of PyH$^{\bullet}$ production. (b) Particle size effect on the PyH$^{\bullet}$ formation kinetics in nonporous silica. Nonporous silica with three different particle sizes (60, 300, and 1000 Å) are used as labeled in the graph.

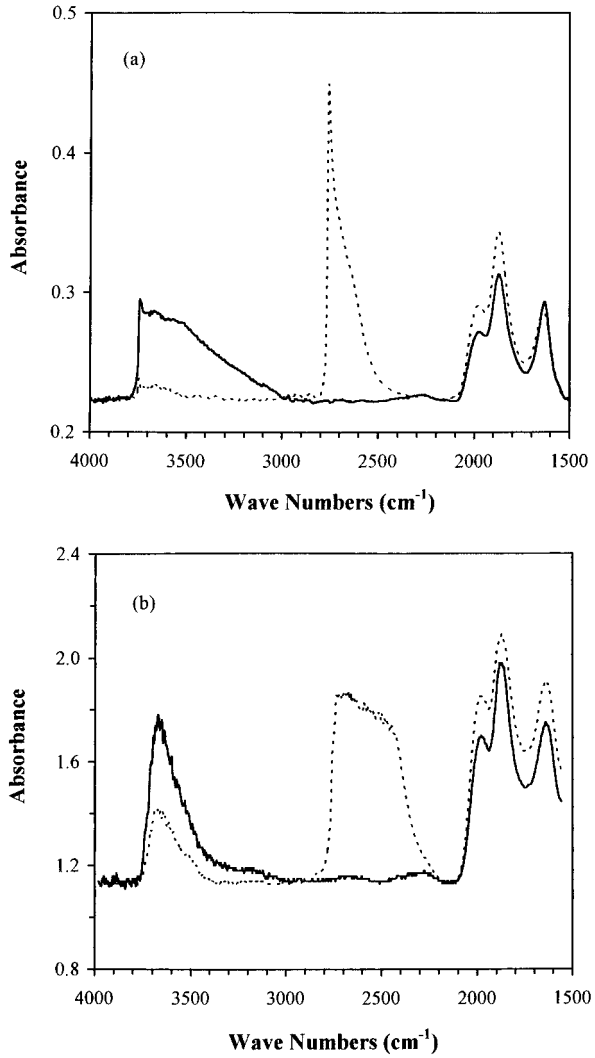

Figure 9. (a) FTIR spectra of a silica gel D60 disc (T_a = 140 °C) before (solid line) and after (dashed line) the hydrogen−deuterium exchange reaction. (b) FTIR spectra of a monospherical silica M1000 disc (T_a = 140 °C) before (solid line) and after (dashed line) the hydrogen−deuterium exchange reaction.

of different silica is clearly observed. From the experimental data, the diffusion constant of H atoms in bulk silica is estimated around 10^{-5} cm^2/s. This is very close to the value previously measured from the hydrogen effect on defect annealing in bulk silica.[52]

3. *N,N*-Dimethylaniline (DMA) on Silica Surface. Organic probe molecules other than pyrene can also be loaded on the silica gel surface and essentially the same chemistry is observed. DMA is particularly useful in the measurement of total transient yields beacuse it can provide complete coverage of the available silica surface. Adsorption isotherms of DMA on silica gel D60 surfaces pretreated at 150 and 600 °C exhibit the same amount of DMA for the monolayer coverage, $[DMA]_m = 7.14 \times 10^{-4}$ mol/g. The transient spectrum of a D60 sample with monolayer coverage by DMA, taken after the decay of the trapped electrons, clearly shows two long-lived absorption bands centered around 370 and 470 nm, respectively (Figure 10). Similar spectra are observed at lower DMA loadings. Introduction of oxygen results in a static quenching of the 370 nm band, leaving the 470 nm band unaffected. The former is assigned to the hydrogen adduct of DMA, and the latter is due to the radical cation of DMA. The absorption spectrum of the H adduct of DMA taken in an aerated MeOH solution with [DMA] = 0.10 M is also shown in Figure 10.

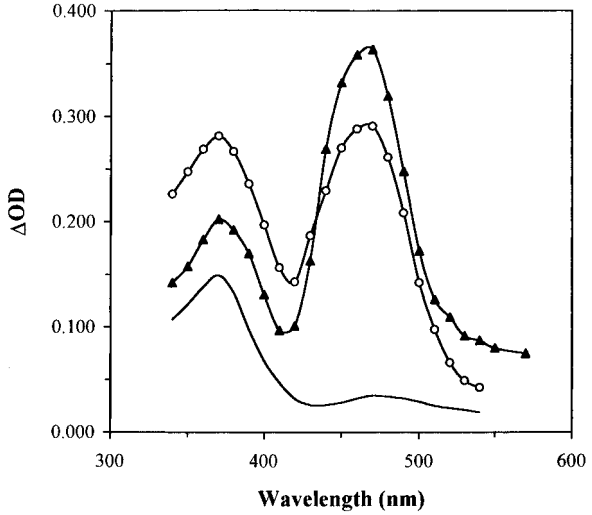

Figure 10. Transient absorption spectra of irradiated D60 powder samples with monolayer DMA coverage (circles, T_a = 140 °C; triangles, T_a = 600 °C), taken at 0.5 μs after the pulse. Absorption spectrum of the H adduct of DMA measured in aerated MeOH with [DMA] = 0.10 M is also shown for comparison (solid line).

$$H + DMA \rightarrow DMAH^{\bullet} \quad (16)$$

$$h^{+}(SiO_2) + DAM \rightarrow DMA^{+\bullet} \quad (17)$$

The same spectrum of the H adduct of DMA with a maximum at 370 nm was reported in cyclohexane and aqueous solutions.[53] The much stronger band at 470 nm observed in the DMA/D60 system, compared to that in liquid methanol, indicates that positive charge transfer from silica to DMA on the surface is a significant process in the radiolysis of silica. Compared with the Py/D60 systems, the relatively lower intensity of the DMAH$^{\bullet}$ radical band is due to its lower extinction coefficient (ϵ = 4000 M^{-1} cm^{-1} at 370 nm) compared to that of DMA$^{+\bullet}$ (ϵ = 12 000 M^{-1} cm^{-1} at 470 nm). The yields of DMAH$^{\bullet}$ and DMA$^{+\bullet}$ in the monolayer-loaded sample are estimated to be G(DMAH$^{\bullet}$) = 4.2 and G(DMA$^{+\bullet}$) = 1.4 for 150 °C pretreated D60. These values give the upper limits of hydrogen production and charge separation in irradiated silica gel D60. Here DMA provides a quantitative measurement of the partition of excitation energy into the free radical process initiated by H atoms and the ionic processes such as charge transfer and electron trapping.

4. Methyl Viologen Adsorbed on Silica Surface. Photoexcitation of methyl viologen (MV^{2+}) on silica gel surfaces leads to an electron transfer reaction giving reduced methyl viologen ($MV^{+\bullet}$) as a product.[54,55] This is easily identified by its UV−visible absorption spectrum. In addition to its well-established electron-scavenging reaction, the hydrogen addition reaction of MV^{2+} has also been characterized in aqueous solution.[56] The addition reaction takes place at two different positions around the pyridine ring, i.e. H addition to either the nitrogen or the ring carbon atoms. The former H adduct quickly transforms into a protonated form of reduced methyl viologen ($MV^{+\bullet}H^{+}$) which exhibits the same absorption spectrum as $MV^{+\bullet}$. The latter H adduct, much like a hydrocyclohexadienyl radical, has a weak absorption band at 470 nm. The H addition to nitrogen is the more preferred reaction path. These characteristic reactions (particularly electron scavenging) enable us to use MV^{2+} as a probe for further examination of the early electronic processes on the silica surface induced by high-energy radiation.

Figure 11a shows a typical transient absorption spectrum of MV^{2+}/D60 taken at 0.2 μs after the electron pulse. Two strong bands at 390 and 590 nm may be assigned to either reduced methyl viologen ($MV^{+\bullet}$) or one of the H adducts of MV^{2+}

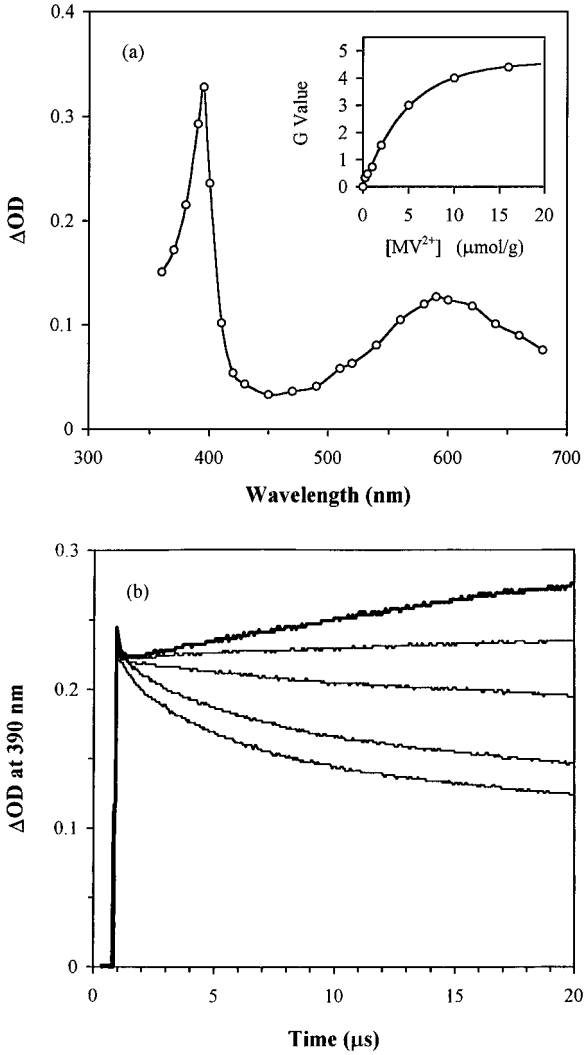

Figure 11. (a) Transient absorption spectrum of an irradiated MV^{2+}/D60 (T_a = 80 °C in vacuum) powder sample, taken at 0.2 μs after the electron pulse. $[MV^{2+}] = 2.0 \times 10^{-6}$ mol/g. Inset: G values of $MV^{+\bullet}$ at different MV^{2+} loadings in silica gel D60. Fitting of the data using a Perrin model for the electron scavenging by MV^{2+} gives a critical radius of 43 Å (smooth line). (b) Oxygen effect on the 390 nm band of the spectrum given in (a). $[MV^{2+}] = 2.0 \times 10^{-6}$ mol/g. The trace taken in vacuum is shown in a thick solid line. The oxygen pressures are 1, 10, 40, and 100 mbar in the order of successive quenching.

($MV^{+\bullet}H^+$), since they have essentially the same spectral shape.[56] At low MV^{2+} loadings, a slow growth of the signal is monitored at 390 nm right after the pulse and is similar to that observed in Py/D60. Introduction of 2 mbar of oxygen completely removes the slow formation over many microseconds, indicating that $MV^{+\bullet}H^+$ is produced from the interpore hydrogen addition reaction in D60 (Figure 11b). Adsorption of pentane from the vapor phase also removes the slow formation and leaves the fast rise component intact. It again confirms the reaction of MV^{2+} with the H atoms.

$$H + MV^{2+} \rightarrow HMV^{2+\bullet} \rightarrow MV^{+\bullet}H^+ \qquad (18)$$

No such slow growth is observed at 470 nm, which suggests that H addition to ring carbon atoms is not favored on a silica surface.

The same strong absorption bands, as shown in Figure 11a, are still present even in a slurry system where the silica pores are filled with cyclohexane. It is known that the rate constant of H + MV^{2+} is 1 order of magnitude slower than that of H + Py in solution.[25,46] If the spectrum is solely due to $MV^{+\bullet}H^+$ from reaction 18, the rate constant should be reduced much more than that of $PyH^\bullet$ in the cyclohexane slurry. In addition, no oxygen quenching is observed for the prompt formation of the 390 nm band up to a pressure of 100 mbar (Figure 11b). All these experiments support the assignment of the immediate component of the spectrum to $MV^{+\bullet}$, which is produced by scavenging the excess electrons from the solid.

$$e^-(\text{conduction band}) + MV^{2+} \rightarrow MV^{+\bullet} \qquad (19)$$

The yields of $MV^{+\bullet}$ measured right after the pulse at different methyl viologen loadings are given in the inset of Figure 11a. A critical electron capture radius of 43 Å is deduced from a three-dimensional Perrin model. As a result of such an efficient electron scavenging by MV^{2+}, H atoms cannot be generated in the vicinity of MV^{2+} sites where the reduction of MV^{2+} is the dominating process. This means that the chance for the intrapore H additon to MV^{2+} is very small. H atoms produced away from the MV^{2+} sites react with MV^{2+} in an interpore fashion by diffusing through the porous structure. It is also observed that the slow component as described in reaction 18 gradually disappears at high MV^{2+} loadings due to the fact that electron scavenging by MV^{2+} completely shuts down the hydrogen production.

5. Effect of Surface Dehydroxylation. As we indicated earlier, thermal treatment at 600 °C removes most of the hydroxyls on the silica surface, leaving only isolated hydroxyls. The same transient intermediates of pyrene are produced on irradiation of the dehydroxylated surface, as illustrated in Figure 3a. A comparison of dehydrated and dehydroxylated silica gel D60 with the same amount of pyrene loading, [Py] = 1.3×10^{-6} mol/g, shows a significant increase in the production of radical ions, i.e. pyrene radical cations and radical anions, and a slight decrease in the yield of $PyH^\bullet$ radicals. The preferential adsorption of pyrene on surface silanol groups and the inability for pyrene to cover the entire silica surface may not be suitable for a quantitative description of the dehydroxylation effect. However, DMA can be used here to measure and compare the yields of radical and ionic products on the surfaces of D60 pretreated at 150 and 600 °C. Figure 10 gives the transient spectra for dehydrated D60 and dehydroxylated D60 with monolayer coverage by DMA. An increase in the yield of DMA cation radicals is indeed observed with less $DMAH^\bullet$ produced on 600 °C dried D60. The G values of DMA transients are measured to be $G(DMAH^\bullet) = 2.9$ and $G(DMA^{+\bullet}) = 1.9$. The drop in the hydrogen production in high-temperature activated silica D60 is attributed to the lower number of hydroxyl groups per unit surface area. The increased cationic product on the dehydroxylated surface is in agreement with the concept of radiation creation of acidic centers in silica by high temperature pretreatment.[11,12]

6. Energy Transfer Mechanism. In low-energy or photochemical studies of high surface area silica, the silica serves only as a solid support, and it is the adsorbed species that are excited and give rise to subsequent chemistry. In the case of high energy radiation, the initial energy loss is to the bulk amorphous SiO_2. Direct excitation of organic adsorbates and hydroxyl groups, which are present as impurities on the silica surface, is negligible. Therefore, the mechanisms of electronic excitation and exciton formation in particulate silica are expected to be the same as those in bulk, amorphous silicon dioxide SiO_2 (i.e. fused quartz). A comparison of experimental studies between these two different areas, i.e. small particles vs bulk materials, clearly demonstrates the significant role that surface plays in controlling the resulting chemistry.

Extensive work on silica materials, particularly in the last 20 years, has been driven by the development of high-purity silica for optical fiber applications. These studies have built up a rather detailed understanding of the electronic excitation and defect formation in SiO_2.[57−65] It is known that band edge and band-to-band excitations of crystalline and amorphous SiO_2, by multiphoton techniques and ionizing radiation, lead to the formation of bound electron−hole pairs, i.e. excitons.[62,63] Free excitons are subject to the self-trapping by structural irregularities (bond length and bond angle) in the Si−O−Si network. The relaxation of the singlet excitons to the triplet state and the adiabatic localization of the triplet excitons occurs rapidly and gives rise, within ∼250 fs, to the self-trapped excitons (STE) in the triplet state.[63] The structure of a self-trapped triplet exciton derived from the atomic displacement on the excited state potential surface was shown to be a partially formed vacancy−interstitial pair with the hole completely localized onto a displaced oxygen (interstitial) and the electron centered at the developing oxygen vacancy.[62−64] This species resembles an *E*′ center−peroxy linkage defect pair. Further adiabatic displacement of the interstitial oxygen atom to a more distant potential minimum results in the formation of a permanent Frenkel defect pair.[64] The correlation between the relaxation of excitons and the formation of STEs,[63] the production of *E*′ centers from the dissocation of the STEs,[62] and the photochemical production of equivalent number of *E*′ centers and peroxy radicals[59] make a convincing case for the creation of lattice defects by excitonic processes. However, the yield of defect production is normally very low, with *G* values on the order of 10^{-3}∼10^{-4}. Although the efficiency of creating the STEs by ionizing radiation was found to be above 0.3 STE per electron−hole pair, i.e. *G*(STE) ≥ 1.5∼1.8, most of the STEs recombine and relax to the ground state radiatively and nonradiatively.[61,62] The nearly complete excitation relaxation with only minor chemical changes makes quartz silica an excellent radiation resistant material.

The division of bulk silica into fine particles of nanometer dimension emphasizes the role that surface plays in the excitation relaxation processes. The free exciton in SiO_2 particles, prior to its self-trapping, could be localized at hydroxyl groups which densely populate the surface. This leads to the breakage of the O−H bond, to the production of hydrogen atoms, and to the formation of NBOHC. Therefore, equation 1 can be detailed as follows.

$$\text{exciton} + \equiv\text{SiO}-\text{H} \rightarrow \equiv\text{SiO}^{\bullet} + \text{H} \qquad (20)$$

These events are especially true for particulate silicas with fully hydroxylated surfaces. The measurement of large *G* values of H adducts on the silica gel surface clearly shows that exciton localization at the surface hydroxyls with subsequent H atom production accounts for ∼75% of radiation chemistry in dehydrated silica gel D60. This process is in competition with the subpicosecond exciton relaxation and self-trapping processes. Such a dramatic surface effect is gradually suppressed with the increasing size of silica particles, as seen from $G(\text{H}) = 4.2$ in D60 to $G(\text{H}) \sim 0.8$ in M1000. The same bond fission process also occurs predominately in wet bulk silica with a hydroxyl content of 1200 ppm.[58] Both atomic hydrogen and NBOHC defects were observed by the ESR technique at low temperatures, and the *G* values are on the order of 10^{-2}∼10^{-3}. A comparison of wet quartz, monospherical M1000, and silica gel D60 clearly shows a gradual transition of radiation chemistry from the inefficient creation of lattice defects in the bulk to the large yields of chemical reactions on the surface.

In view of the large yield of H atoms produced in reaction 20, we speculate that the same amount of ≡SiO• should be left on the irradiated surface. A red absorption band has been previously attributed to the NBOHC in irradiated or drawn silica fibers.[60] However, it is too weak to be detected optically in our experiments, since its extinction coefficient is only 60 M^{-1} cm^{-1}. There is enough evidence to show that the very short-lived strong absorption around 600 nm in Figure 1a is not due to the NBOHC. The fate of ≡SiO• on the surface and its chemical consequences in surface modification[10] are to be further examined.

Another interesting aspect of the surface effect on the excitation relaxation involves charge trapping by species present on silica surfaces. Recent experimental studies have attributed electron trapping in amorphous silica to the pre-existing defects, such as peroxy radicals and precursors of *E*′ centers.[66]

$$e^- + SiO_2 \rightarrow E_{tr}^- \text{ (long-lived)} \qquad (21)$$

The trapping of excess electrons at energy levels deep in the band gap accounts for the stability of E_{tr}^- in bulk silica as shown in the charging measurements.[66] The presence of a fully hydroxylated surface on the silica particles introduces new electron trapping sites. These involve multiple hydroxyl groups on the surface and are identified in this study.

$$e^- + (\equiv\text{SiOH})_n \rightarrow e_{tr}^- \ (\lambda_{max} = 600 \text{ nm}, \tau_{1/2} \sim 50 \text{ ns}) \qquad (22)$$

The efficient photoionization of aromatic adsorbates such as pyrene on silica surfaces results from both of the above trapping modes. The slow ion recombination over milliseconds and seconds in both photolysis and radiolysis experiments suggests that the fast decay of e_{tr}^-, which is independent of the aromatic radical cations, might be due to its transformation into deeper traps in the bulk as described in equation 21. The low yields of pyrene anion radicals on silica surfaces pretreated at 150 and 600 °C also indicate that most of the excess electrons are trapped by silica rather than scavenged by pyrene. However, the presence of strong electron acceptors such as $CHCl_3$, Cd^{2+}, and MV^{2+} results in efficient scavenging of conduction band electrons before formation and localization of excitons. The electron affinity of silica is thus determined to be higher than that of biphenyl or pyrene but lower than that of $CHCl_3$ or MV^{2+}. Meanwhile, charge transfer reactions of organic adsorbates with liberated holes left in the SiO_2 network give rise to the increased production of radical cations. In a fashion similar to hydrogen production from the O−H bond breakage via exciton localization, the efficiency of these charge-scavenging reactions drops on increasing the size of the primary silica particles. This is due to the shielding of the bulk SiO_2 from electronic interaction with adsorbed species.

The dramatic effect of the surface on electronic excitation in silica is further evident when a fully hydroxylated surface is modified by pretreatment at high temperatures. As a result of dehydroxylation, less H atoms are produced with more electron−hole pairs subject to scavenging. This leads to a shift of energy transfer to the ion radical channel and therefore ionic chemistry on silica surfaces. This explains the previous observation of acidic center formation on high temperature activated silica surfaces and reactions initiated by a cationic mechanism. It is noted that about 50% of the excitation energy goes into hydrogen production in silica gel dried at 600 °C. This is in spite of the fact that its hydroxyl content is only 10 times higher than that in wet quartz where the hydrogen yield is as low as $G(\text{H}) \sim 10^{-2}$.

The radiation-induced energy transfer processes in high surface area silicas are summarized in the following sentences. The primary form of energy exists as unrelaxed electron−hole

pairs in the amorphous SiO_2 particles. The splitting of the electron−hole pairs by the intrinsic charge-trapping centers and the charge-scavenging molecules adsorbed on the surface competes with the formation of excitons. The localization of the excitons at surface hydroxyls leads to instantaneous H atom production. The variation of the surface chemistry originates from the modulation of the hydroxyl content which is present as an impurity within the band gap. In silicas of small particle structures such as silica gels, surface hydroxyls withdraw the energy via exciton trapping and direct the chemistry of adsorbates into free radical processes. Meanwhile, dehydroxylation of the surface switches the mode of energy transfer from radical to ionic in nature.

It is useful to comment on the radiolysis of other similar structures, namely zeolites. The particle-based structure of silica is different from the zeolite framework which is interpenetrated by cage structures on the atomic level and therefore completely exposed to external ions and small molecules. The presence of Na^+ clusters as intrinsic electron-trapping sites and water clusters as externally introduced electron traps in zeolite cavities leads to a very efficient charge separation upon high-energy excitation of the zeolite framework. Therefore, ionic processes are mainly observed in zeolites.[23]

Conclusion

Upon high-energy irradiation, hydrogen atoms and hydrogen gas are produced with significant yields on silica surfaces. Trapping of free charge carriers leads to the observation of surface-trapped electrons and holes in hydroxylated and dehydroxylated silicas, respectively. The formation of the H adducts and radical ions of aromatic adsorbates was observed simultaneously with the reduction of the hydrogen gas yield on the 140 °C dried silica surface. The hydrogen atoms are shown to be the precursor of molecular hydrogen and the H adducts. The adsorption of aromatic molecules preferentially at the hydroxyl rich sites on silica surfaces facilitates the H addition reactions. *G* value measurements suggest that the hydrogen production is the major radiolytic process on the fully hydroxylated silica surface. Dehydroxylation by sample pretreatment at 600 °C leads to a decreased yield of the H adducts and increased yields of radical ions.

The mechanisms of energy transfer and formation of the reactive intermediates of organic adsorbates on silica surfaces are discussed and correlated with the small particle based structures of the high surface area silicas used in the studies. The hydroxyl impurities present on silica surfaces are found to be the most important factor in directing the surface chemistry into radical or ionic channels via modulation of the excitation transfer from inside the primary SiO_2 particles. These surface reactions are less readily observed with increasing size of silica particles. This is indicative of a gradual transition of radiation chemistry from the surface to the bulk.

Acknowledgment. The authors are grateful to the National Science Foundation for financial support of this work. We also want to thank the Radiation Laboratory, University of Notre Dame, for use of the ^{60}Co γ source.

References and Notes

(1) Rabe, J. G.; Rabe, B.; Allen, A. O. *J. Am. Chem. Soc.* **1964**, *86*, 3887; *J. Phys. Chem.* **1966**, *70*, 1098.

(2) Sutherland, J. W.; Allen, A. O. *J. Am. Chem. Soc.* **1961**, *83*, 1040. Abrams, L.; Allen, A. O. *J. Phys. Chem.* **1969**, *73*, 2741.

(3) Hentz, R. R. *J. Phys. Chem.* **1962**, *66*, 1625. Hentz, R. R.; Wickenden, D. K. *J. Phys. Chem.* **1969**, *73*, 817.

(4) Kohn, H. W. *J. Phys. Chem.* **1962**, *66*, 1185; *J. Phys. Chem.* **1964**, *68*, 3129.

(5) Sagert, N. H.; Dyne, P. J. *Can. J. Chem.* **1967**, *45*, 615.

(6) Shimada, M.; Nakamura, Y.; Kusama, Y.; Udagawa, A.; Takehisa, M. *J. Appl. Polym. Sci.* **1982**, *27*, 1259.

(7) Bruk, M. A.; Pavlov, G. G. Isaeva; Yunitskaya, E. Ya. *Eur. Polym. J.* **1986**, *22*, 169.

(8) Emmett, P. H.; Livingston, R.; Zeldes, H.; Kokes, R. J. *J. Phys. Chem.* **1962**, *66*, 921.

(9) Kazansky, V. B.; Pariisky, G. B.; Voevodsky, V. V. *Discuss. Faraday Soc.* **1962**, *31*, 203.

(10) Tagieva, M. M.; Kiselev, V. F. *Rus. J. Phys. Chem.* **1961**, *35*, 680.

(11) Rojo, E. A.; Hentz, R. R. *J. Phys. Chem.* **1966**, *70*, 2919.

(12) Barter, C.; Wagner, C. D. *J. Phys. Chem.* **1964**, *68*, 2381; *J. Phys. Chem.* **1965**, *69*, 491.

(13) Wong, P. K.; Willard, J. E. *J. Phys. Chem.* **1968**, *72*, 2623. Joppien, G. R.; Willard, J. E. *J. Phys. Chem.* **1972**, *76*, 3158.

(14) Wong, P. K.; Allen, A. O. *J. Phys. Chem.* **1970**, *74*, 774.

(15) Bauer, R. K.; de Mayo, P.; Ware, W. R.; Wu, K. C. *J. Phys. Chem.* **1982**, *86*, 3781. Bauer, R. K.; Borenstein, R.; de Mayo, P.; Okada, K.; Rafalska, M.; Ware, W. R.; Wu, K. C. *J. Am. Chem. Soc.* **1982**, *104*, 4635.

(16) Turro, N. J.; Cheng, C. C.; Mahler, W. *J. Am. Chem. Soc.* **1984**, *106*, 5022. Turro, N. J.; Zimmt, M. B.; Gould, I. R. *J. Am. Chem. Soc.* **1985**, *107*, 5826.

(17) Oelkrug, D.; Fleming, W.; Fulleman, R.; Gunther, R.; Honnen, W.; Krabichler, G.; Schafer, M.; Uhl, S. *Pure Appl. Chem.* **1986**, *58*, 1207. Oelkrug, D.; Reich, S.; Wilkinson, F.; Leicester, P. A. *J. Phys. Chem.* **1991**, *95*, 270.

(18) Hite, P.; Kransnansky, R.; Thomas, J. K. *J. Phys. Chem.* **1986**, *90*, 5765. Kransnansky, R.; Koike, K.; Thomas, J. K. *J. Phys. Chem.* **1990**, *94*, 4521.

(19) Thomas, J. K. *The Chemistry of Excitation at Interfaces*; *ACS Monograph Series* 181; American Chemical Society: Washington, DC, 1984.

(20) Thomas, J. K. *Chem. Rev.* **1993**, *93*, 301.

(21) Thomas, J. K. *J. Phys. Chem.* **1987**, *91*, 267.

(22) Kalyanasundaram, K. *Photochemistry in Organized and Constrained Media*; Ramamurthy, V., Ed.; VCH.: New York, 1991; Chapter 2.

(23) Liu, X.; Zhang, G.; Thomas, J. K. *J. Phys. Chem.* **1995**, *99*, 10024; *J. Phys. Chem. B* **1997**, *101*, 2181.

(24) Mao, Y.; Iu, K.-K.; Thomas, J. K. *Langmuir* **1994**, *10*, 709.

(25) Zhang, G.; Thomas, J. K. *J. Phys. Chem.* **1994**, *98*, 11714.

(26) Zhang, G.; Thomas, J. K. *J. Phys. Chem.* **1996**, *100*, 11438.

(27) Iler, R. K. *The Chemistry of Silica: Solubility, Polymerization, Collod and Surface Properties, and Biochemistry*; John Wiley & Sons: New York, 1979.

(28) Adamson, A. W. *Physical Chemistry of Surfaces*, 5th ed.; John Wiley & Sons: New York, 1990; Chapter 11.

(29) Richards, J. T.; Thomas, J. K. *J. Chem. Phys.* **1970**, *53*, 218.

(30) Pauly, S. In *Polymer Handbook*, 3rd ed.; Brandrup, J., Immergut, E. H., Eds.; John Wiley & Sons: New York, 1989; Chapter 6.

(31) Zhang, G. Radiation Induced Processes in Polymer Films and on Silica Surfaces. Ph.D. Dissertation, University of Notre Dame, Indiana, 1996.

(32) Wertz, J. E.; Bolton, J. R. *Electron Spin Resonance: Elementary Theory and Practical Applications*, Capman Hall: New York, 1986.

(33) Silin, A. R.; Skuja, L. N. *J. Mol. Struct.* **1980**, *61*, 145. Griscom, D. L. J. *Non-Cryst. Solids* **1985**, *73*, 51.

(34) Nicollian, E. H.; Brews, J. R. *Metal Oxide Semiconductor Physics and Technology*; John Wiley & Sons: New York, 1982; Chapter 11.

(35) Mao, Y.; Thomas, J. K. *J. Phys. Chem.* **1995**, *99*, 2048.

(36) Griscom, D. L. J. *Non-Cryst. Solids* **1984**, *68*, 301.

(37) Zhang, G.; Thomas, J. K. Unpublished results.

(38) Nelson, C. M.; Week, R. A. *J. Am. Ceram. Soc.* **1960**, *43*, 396. Friebele, E. J.; Higby, P. L.; Cai, T. E. *Diffus. Defect Data* **1987**, *53−54*, 203.

(39) Samuel, J.; Ottolenghi, M.; Avnir, D. *J. Phys. Chem.* **1992**, *96*, 6398.

(40) Mao, Y.; Thomas, J. K. *Chem. Phys. Lett.* **1994**, *226*, 127.

(41) Zhang, G.; Thomas, J. K. Unpublished results. In contrast to the very fast H addition to pyrene in acidic methanol (within 5 ns), protonation of the pyrene anion radical ($H^+ + Py^{-\bullet}$) occurs over several hundred nanoseconds in pulse radiolysis of neutral methanol.

(42) Okada, T.; Mori, T.; Mataga, N. *Bull. Chem. Soc. Jpn* **1976**, *49*, 3398. Okada, T.; Tashita, N.; Mataga, N. *Chem. Phys. Lett.* **1980**, *75*, 220. Okada, T.; Karaki, I.; Mataga, N. *J. Am. Chem. Soc.* **1982**, *104*, 7191.

(43) Elliot, S. R. *Physics of Amorphous Materials*, 2nd ed.; Longman Scientific & Technical: England, 1990; Chapter 6.

(44) Hsu, K.-J.; Anderson, S. M.; Durant, J. L.; Kaufman, F. *J. Phys. Chem.* **1989**, *93*, 1018.

(45) Dixon-Lewis, G.; Williams, D. J. In *Comprehensive Chemical Kinetics*, Vol. 17: *Gas-Phase Combustion*, Bamford, C. H., Tipper, C. F. H., Compton, R. G., Eds.; Elsevier: Amsterdam, 1977; Chapter 1.

(46) Buxton, G. V.; Greenstock, C. L.; Helman, W. P.; Ross, A. B. *J. Phys. Chem. Ref. Data* **1988**, *17*, 513.

(47) Sauer, M. C., Jr.; Ward, B. *J. Phys. Chem.* **1967**, *71*, 3971.

(48) Abell, P. I. *Comprehensive Chemical Kinetics, Vol.18: Selected Elementary Reactions*; Bamford, C. H.; Tipper, C. F. H., Eds.; Elsevier: Amsterdam, 1976; Chapter 3.

(49) Technical data of monospherical silica from E. Merck Industries, Inc.

(50) Benesi, H. A.; Jones, A. C. *J. Phys. Chem.* **1959**, *63*, 179.

(51) Davydov, V. Ya.; Kiselev, A. V.; Zhuravlev, L. T. *Trans. Faraday Soc.* **1964**, *60*, 2254.

(52) Cai, T. E.; Griscom, D. L.; Friebele, E. J. *Phys. Rev. B* **1989**, *40*, 6374.

(53) Christensen, H. *Int. J. Radiat. Phys. Chem.* **1972**, *4*, 311. Zador, E.; Warman, J. M.; Hummel, A. *J. Chem. Soc., Faraday Trans. 1* **1976**, *72*, 1368.

(54) Mao, Y.; Thomas, J. K. *J. Phys. Chem.* **1995**, *99*, 9909.

(55) Xiang, B.; Kevan, L. *J. Phys. Chem.* **1994**, *98*, 5120.

(56) Solar, S.; Solar, W.; Getoff, N. *J. Chem. Soc., Faraday Trans. 1* **1984**, *80*, 2929. Solar, S.; Solar, W.; Getoff, N.; Holcman, J.; Sehested, K. *J. Chem. Soc., Faraday Trans. 1* **1982**, *78*, 2467.

(57) Griscom, D. L. *J. Ceram. Soc. Jpn.* **1991**, *99*, 923 and references therein.

(58) Friebele, E. J.; Griscom, D. L.; Stapelbroek, M.; Weeks, R. A. *Phys. Rev. Lett.* **1979**, *42*, 1346. Stapelbroek, M.; Griscom, D. L.; Friebele, E. J.; Sigel, G. H. *J. Non-Cryst. Solids* **1979**, *32*, 313.

(59) Tsai, T. E.; Griscom, D. L.; Friebele, E. J. *Phys. Rev. Lett.* **1988**, *61*, 444. Devine, R. A. B. *Phys. Rev. Lett.* **1989**, *62*, 340.

(60) Hibino, Y.; Hanafusa, H.; *J. Appl. Phys.* **1986**, *60*, 1797. Friebele, E. J.; Sigel, G. H.; Griscom, D. L. *Appl. Phys. Lett.* **1979**, *32*, 313.

(61) Hayes, W.; Kane, M. J.; Salminen, O.; Wood, R. L.; Doherty, S. *J. Phys. C* **1984**, *17*, 2943. Fisher, A. J.; Hayes, W.; Stoneham, A. M. *Phys. Rev. Lett.* **1990**, *64*, 2667.

(62) Tanimura, K.; Tanaka, T.; Itoh, N. *Phys. Rev. Lett.* **1983**, *51*, 423. Tanimura, K.; Itoh, C.; Itoh, N. *J. Phys. C.* **1988**, *21*, 1869. Itoh, C.; Tanimura, K.; Itoh, N. *J. Phys. C.* **1988**, *21*, 4693. Itoh, C.; Suzuki, T.; Itoh, N. *Phys. Rev. B* **1990**, *41*, 3794.

(63) Saeta, P. N.; Greene, B. I. *Phys. Rev. Lett.* **1993**, *70*, 3588. Audebert, P.; Daguzan, P.; Dos Santos, A.; Gauthier, J. C.; Geindre, J. P.; Guizard, S.; Hamoniaux, G.; Krastev, K.; Martin, P.; Petite, G.; Antonetti, A. *Phys. Rev. Lett.* **1994**, *73*, 1990.

(64) Shluger, A. L. *J. Phys. C* **1988**, *21*, L431. Shluger, A. L. Stefanovich, E. *Phys. Rev. B* **1990**, *42*, 9664.

(65) Song, K. S.; Williams, R. T. *Self Trapped Excitons*, 2nd ed.; Springer Series in Solid State Sciences 105; Springer-Verlag: Berlin, 1996; Chapter 7.

(66) Vigouroux, J. P.; Durand, J. P.; LeMoel, A.; Le Gressus, C.; Griscom, D. L. *J. Appl. Phys.* **1985**, *57*, 5139.